Review Article

4D flow imaging with MRI

Zoran Stankovic[1], Bradley D. Allen[1], Julio Garcia[1], Kelly B. Jarvis[1], Michael Markl[1,2]

[1]Department of Radiology, Feinberg School of Medicine, Northwestern University, Chicago, USA; [2]Department Biomedical Engineering, McCormick School of Engineering, Northwestern University, Chicago, USA

Correspondence to: Michael Markl, PhD. Department of Radiology, Northwestern University, 737 N. Michigan Avenue Suite 1600, Chicago, Illinois 60611, USA. Email: michael.markl@northwestern.edu.

Abstract: Magnetic resonance imaging (MRI) has become an important tool for the clinical evaluation of patients with cardiovascular disease. Since its introduction in the late 1980s, 2-dimensional phase contrast MRI (2D PC-MRI) has become a routine part of standard-of-care cardiac MRI for the assessment of regional blood flow in the heart and great vessels. More recently, time-resolved PC-MRI with velocity encoding along all three flow directions and three-dimensional (3D) anatomic coverage (also termed '4D flow MRI') has been developed and applied for the evaluation of cardiovascular hemodynamics in multiple regions of the human body. 4D flow MRI allows for the comprehensive evaluation of complex blood flow patterns by 3D blood flow visualization and flexible retrospective quantification of flow parameters. Recent technical developments, including the utilization of advanced parallel imaging techniques such as k-t GRAPPA, have resulted in reasonable overall scan times, e.g., 8-12 minutes for 4D flow MRI of the aorta and 10-20 minutes for whole heart coverage. As a result, the application of 4D flow MRI in a clinical setting has become more feasible, as documented by an increased number of recent reports on the utility of the technique for the assessment of cardiac and vascular hemodynamics in patient studies. A number of studies have demonstrated the potential of 4D flow MRI to provide an improved assessment of hemodynamics which might aid in the diagnosis and therapeutic management of cardiovascular diseases. The purpose of this review is to describe the methods used for 4D flow MRI acquisition, post-processing and data analysis. In addition, the article provides an overview of the clinical applications of 4D flow MRI and includes a review of applications in the heart, thoracic aorta and hepatic system.

Keywords: 4D flow magnetic resonance imaging (4D flow MRI); phase contrast magnetic resonance imaging (PC-MRI); blood flow; hemodynamics; PC-VIPR; visualization; quantification; carotid bifurcation; aorta; heart; pulmonary arteries; renal arteries; liver hemodynamics; splanchnic vessel system; peripheral arteries

Submitted Sep 04, 2013. Accepted for publication Oct 21, 2013.
doi: 10.3978/j.issn.2223-3652.2014.01.02
View this article at: http://www.thecdt.org/article/view/3630/4523

Introduction

MR imaging is widely accepted by clinicians as a valuable tool for diagnosing cardiac and vascular diseases, measuring disease severity and assessing patient response to medical and surgical therapy. The technique has been further developed over the last few decades to provide not only morphological information on cardiovascular anatomy, but also functional information on cardiac perfusion, myocardial viability, and blood flow. This functional information may allow a more thorough assessment of cardiovascular diseases.

Since its original description in the 1980s (1-4), phase contrast (PC) magnetic resonance imaging (MRI) has seen broad clinical acceptance for the visualization and quantitative evaluation of blood flow in the heart, aorta and large vessels (5-7). Further development of PC techniques have allowed for the acquisition of a time-resolved (CINE), three-dimensional (3D) PC-MRI with three-directional velocity encoding which is often referred to as "4D flow MRI". In contrast to standard 2D CINE PC-MRI which allows for the evaluation of blood flow in a single user selected 2D slice, 4D flow MRI can provide information

on the temporal and spatial evolution of 3D blood flow with full volumetric coverage of any cardiac or vascular region of interest. A particular advantage over 2D CINE PC-MRI is related to the possibility for retrospective selection of territories at any location inside the 3D data volume to perform *post-hoc* quantification of blood flow parameters such as total flow, peak velocity or regurgitant fraction (8-12). Moreover, the combination of 3D blood flow visualization with flow quantification enables a new and previously unfeasible comprehensive evaluation of the impact of cardiovascular pathologies on global and local changes in cardiac or vascular hemodynamics (13-19).

A number of 4D flow MRI studies have attempted to assess and corroborate blood flow parameters associated with clinical markers commonly measured with Doppler ultrasound (US) and echocardiography: peak pressure gradient ($r=0.96$, $P<0.05$) (20), peak and mean velocities ($r=0.83$ and $r=0.76$, respectively) (21), net flow over the cardiac cycle, vessel area, etc. However, 4D flow MRI can also provide the opportunity to improve upon current clinical hemodynamic assessments by deriving additional metrics of cardiovascular hemodynamics. A number of groups have shown that 4D flow MRI can be used to derive advanced hemodynamic measures such as wall shear stress (WSS) (22-24), pressure difference (20,25-27), pulse wave velocity (28,29), turbulent kinetic energy (TKE) and others (30,31) for an improved characterization of cardiovascular disease beyond simple measures of flow.

The purpose of this review is to provide a brief introduction to the imaging techniques used to acquire 4D flow MRI data as well as the analysis tools currently used for blood flow visualization and flow quantification. Furthermore, a selected number of clinical applications will be presented to illustrate the potential of 4D flow MRI for an improved and more comprehensive evaluation of cardiovascular disease.

Data acquisition methods: from 2D PC to 4D flow MRI

Standard 2D PC-MRI

PC MRI (also sometimes termed 'flow-sensitive MRI' or 'MR velocity mapping') takes advantage of the direct relationship between blood flow velocity and the phase of the MR signal that is acquired during a MRI measurement. To eliminate unwanted background phase effects, two acquisitions with different velocity-dependent signal phase are typically needed to encode (using bipolar magnetic field gradients) and measure blood flow velocity along a single direction (5,32,33). Subtracting of phase images from the two acquisitions removes background phase effects. The signal intensities in the resulting phase difference images are directly related to the blood flow velocity and can thus be used to visualize and quantify blood flow (PC principle).

For cardiovascular applications, the 2D PC data is acquired over multiple cardiac cycles using ECG gated CINE imaging to measure time-resolved pulsatile blood flow as illustrated in *Figure 1*. For a standard 2D CINE PC-MRI clinical protocol, the 2D imaging slice is usually positioned normal to the vessel lumen. Data acquisition typically includes single-direction velocity measurement orthogonal to the 2D imaging slice (through-plane encoding) and is performed during a 10-20-second breath hold period. For certain patients, e.g., patients with congestive heart failure and shortness of breath, this length of breath-hold may not be possible, and is a potential limitation of the clinical implementation of cardiovascular MR. Following image reconstruction, 2D CINE PC-MRI yields a series of anatomical (magnitude) and flow velocity (phase difference) images that represent the temporal changes of morphology and blood flow over the cardiac cycle. Typical measurement parameters are: spatial resolution, 1.5-2.5 mm; temporal resolution, 30-60 ms; slice thickness, 5-8 mm.

PC-MRI and velocity encoding sensitivity (Venc)

An important (user-defined) PC-MRI parameter is the Venc, which represents the maximum flow velocity that can be acquired (*Figure 1*). As shown in *Figure 2*, when the underlying velocity exceeds the acquisition setting for Venc, velocity aliasing can occur which is typically visible as a sudden change from high to low velocity within a region of flow. If aliasing artifacts are present, accurate flow visualization and quantification may be compromised unless antialiasing correction can be successfully performed (34). Alternatively, the Venc can be increased and the acquisition is repeated to avoid aliasing. It is important to note, however, that velocity noise is directly related to the Venc (5). Therefore, selecting a high Venc may alleviate the issue of velocity aliasing but will also increase the level of velocity noise in flow velocity images. As a result, the Venc should ideally be selected as high as needed to avoid aliasing but as low as possible to reduce velocity noise. As a general rule, to capture the best image quality, the chosen Venc should represent the physiological velocity of the vessel of interest and be adapted to the measurement of interest and present hemodynamic conditions. Typical settings for

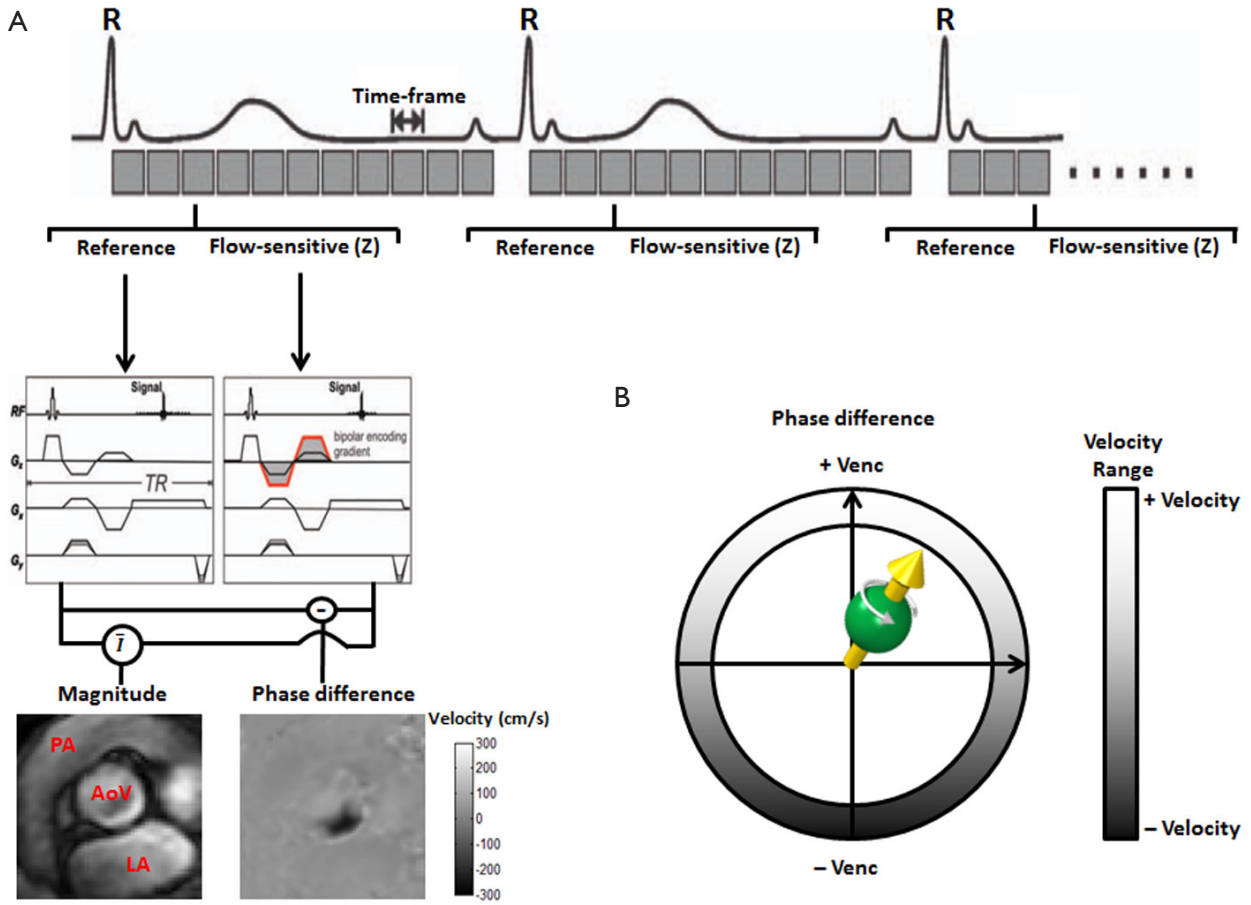

Figure 1 Standard 2D CINE PC-MRI with one-directional through-plane (Z) velocity encoding. (A) Data acquisition is synchronized with the RR-interval by ECG gating. For each cardiac time frame, a reference and velocity sensitive scan (bipolar encoding gradient) are acquired in direct succession. Magnitude images are calculated by averaging both scans. Subtraction of phase images provides phase difference images that contain quantitative blood flow velocities, as shown in a 2D slice above and parallel to the AoV, PA and LA. Due to time constraints, the MR data cannot be acquired during a single heartbeat, thus velocity data are collected over several cardiac cycles; (B) The selection of Venc is necessary for a proper flow measurement. Phase differences in an angle range from $-\pi$ to $+\pi$ or from +Venc to –Venc, defining the velocity range. Blood flow velocities in the predominant blood flow direction will appear bright and blood flow velocities in the opposite direction will appear dark. Note that velocities exceeding Venc results in velocity aliasing as shown in *Figure 2*. MRI, magnetic resonance imaging; AoV, the aortic valve; PA, pulmonary artery; LA, left atrium. Venc, velocity encoding sensitivity.

Venc are: 150-200 cm/s in the thoracic aorta, 250-400 cm/s in the aorta with aortic stenosis or coarctation, 100-150 cm/s for intra-cardiac flow, 50-80 cm/s in large vessels of the venous system. If a large imaging volume with various vessels is examined there may be no optimal Venc setting and the value has to be chosen in accordance to the clinical question.

4D flow MRI

In 4D flow MRI, velocity is encoded along all three spatial dimensions throughout the cardiac cycle, thus providing a time-resolved 3D velocity field (5,35,36). As described above, quantitative velocity measurements require two acquisitions and a subtraction for one-directional velocity encoding. Three-directional velocity measurements can be efficiently achieved by interleaved four-point velocity encoding which acquires one reference image and three velocity-encoded images along three orthogonal (x, y, z) directions (32,37,38). As for 2D CINE PC-MRI, data acquisition is synchronized with the cardiac cycle and data collection is distributed over multiple cardiac cycles using

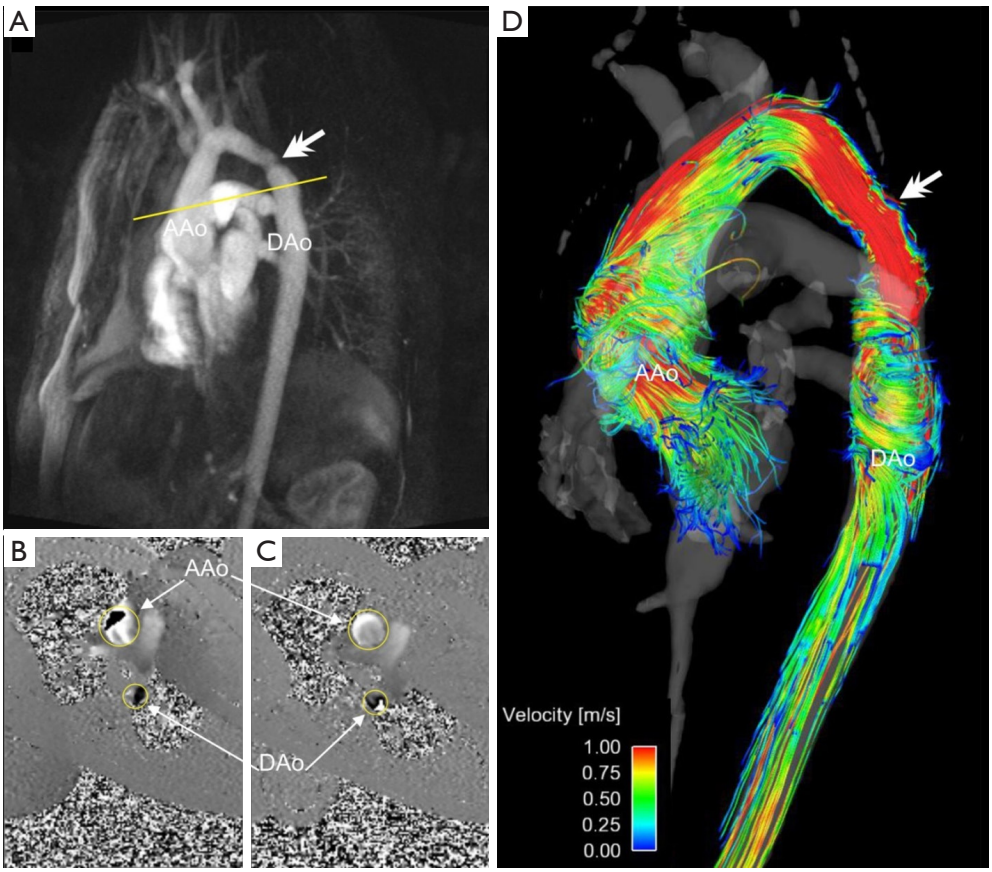

Figure 2 (A-C) 2D CINE PC-MRI with aliasing in a patient with bicuspid aortic valve disease and aortic coarctation. The patient underwent standard MR angiography (A) as well as 2D CINE PC-MRI (B and C) for the quantification of ascending aorta and post-coarctation flow velocity. Velocity aliasing due to blood flow velocities exceeding Venc can be seen within the AAo early in the cardiac cycle in (B), and again in the DAo distal to the coarctation (double white arrow) later in the cardiac cycle. The yellow line in A shows the imaging plane for 2D CINE PC-MRI acquisitions in (B) and (C); (D) 4D flow MRI with improved Venc settings and anti-aliasing corrections allowed for accurate 3D blood flow visualization without aliasing. Flow quantification based on 4D flow MRI revealed a peak velocity of 2.04 m/s in the mid-ascending aorta and 3.49 m/s in the DAo just distal to the coarctation. MRI, magnetic resonance imaging; AAo, ascending aorta ; DAo, descending aorta.

so called ''k-space segmentation' techniques (only a fraction of the entire 4D flow data is measured during each cardiac cycle, the data is successively collected over multiple RR-intervals). After completion of the 4D flow acquisition, four time-resolved (CINE) 3D datasets are generated ('magnitude' data depicting anatomy and three flow datasets representing velocities 'Vx, Vy, and Vz'). For a schematic illustration of the data acquisition process see *Figure 3*.

Due to the large amount of data that has to be collected (three spatial dimensions, three velocity directions, time over the cardiac cycle), efficient data acquisition is necessary to achieve practical scan times for 4D flow MRI in clinical applications. Several recent developments have allowed for marked scan time reductions. From a hardware point of view, the availability of high performance gradients has reduced both the echo and repetition times TE and TR and thereby total scan time. The introductions of phased-array coils, multi-receiver channels, and parallel imaging technology have also been applied to PC-MRI, primarily to reduce the scan time. Other methodological improvements include the use of advanced accelerated imaging approaches such as radial undersampling, kt-BLAST, kt-SENSE, kt-GRAPPA, or compressed sensing (39-42).

For typical cardiovascular applications, scan times between 5 and 20 minutes can be achieved depending on heart rate, spatio-temporal resolution and anatomic

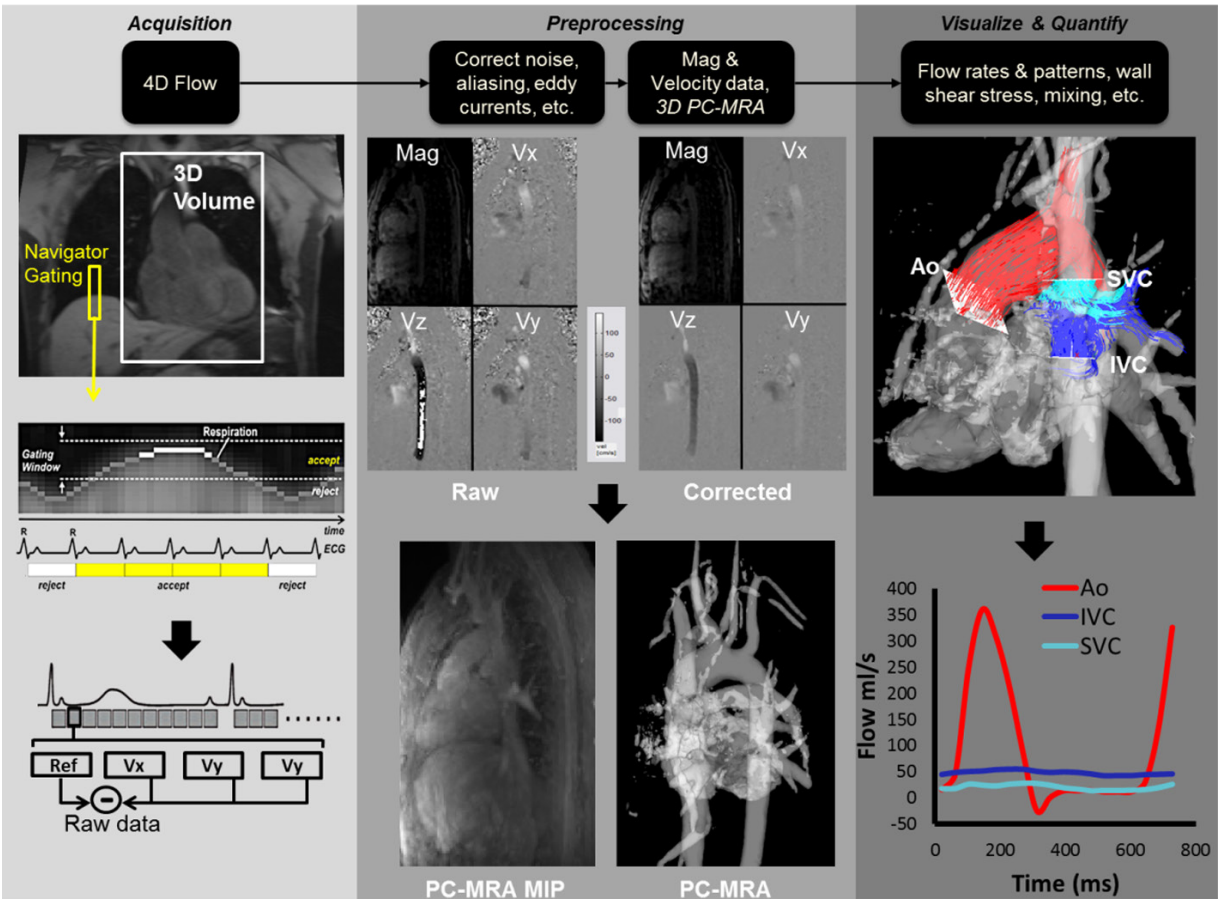

Figure 3 Data acquisition and analysis workflow for 4D flow MRI. (Left) 4D flow MRI data covering the whole heart (white rectangle) is acquired using ECG gating and respiratory control using diaphragm navigator gating. 3D velocity-encoding is used to obtain velocity-sensitive phase images which are subtracted from reference images to calculate blood flow velocities along all three spatial dimensions (Vx, Vy, Vz). (Middle) Data preprocessing corrects for errors due to noise, aliasing and eddy currents and calculates the 3D-PC-MRA. (Right) 3D Blood flow is visualized by emitting time resolved pathlines from analysis planes in the Ao, IVC and SVC. In addition, retrospective quantitative analysis can be used to derive flow-time curves at user selected regions of interest in the cardiovascular system. MRI, magnetic resonance imaging; Ao, aorta; IVC, inferior vena cava; SVC, superior vena cava.

coverage. For thoracic and abdominal applications, respiration control is thus needed to minimize breathing artifacts. Different strategies including respiratory bellows, navigator gating (see *Figure 3*) or self-gating techniques have been applied (43-45).

An alternative technique that is increasingly used to accelerate 4D flow MRI is radial data sampling combined with undersampling [e.g., PC-VIPR, vastly undersampled isotropic projection reconstruction (46)]. Radial acquisition schemes have been shown to permit 4D flow imaging with improved scan time while providing large spherical volumetric coverage with high spatial resolution. Furthermore, PC-VIPR can reduce the occurrence of motion artifacts and enable self-gating due to intrinsic properties of radial data acquisition strategies (47).

Data analysis—preprocessing and corrections

There are multiple sources of phase offset errors in PC and 4D flow MRI that can degrade image quality and impair measurements by introducing inaccuracies in flow quantification. The most commonly encountered inaccuracies include phase offset errors due to eddy currents (48), Maxwell terms (49), and gradient field

nonlinearity (50). A detailed description and discussion of these sources of phase-offset errors is beyond the scope of this review article. Nonetheless, it is important to apply appropriate correction strategies to compensate for these potential sources of error before further processing of the data for 3D visualization or flow quantification. While correction for Maxwell terms and gradient field non-linearity can be performed during image reconstruction (without the need for user interaction), eddy current correction cannot easily be automated and has to be integrated into the data analysis workflow.

The most commonly employed strategy for eddy current correction is based on the methodology presented by Walker *et al*. in 1993 (48). The approach is based on thresh-holding to identify regions with static tissue. These regions are then used to estimate eddy current induced linearly varying phase offset errors which are subsequently subtracted from the entire image. An alternative strategy requires the scanning of a large spherical (static) phantom directly after the 4D flow scan with identical imaging parameters followed by the subtraction of the resulting phase difference images from the *in vivo* 4D flow data. However, the long scan time and logistics needed to perform the additional 4D flow phantom scan make this option less desirable and image based correction is most often used. Unfortunately, no unified strategies, algorithms or software across different MR system vendors and 4D flow MRI applications exist. Nevertheless, studies have shown that 4D flow MRI can be reliably used for 3D visualization and flow quantification if appropriate correction strategies such as proposed by Walker *et al*. (48) are employed (see also *Figure 3* for 4D flow analysis workflow including eddy current and velocity aliasing corrections).

Data analysis—3D phase contrast MR angiography (3D PC-MRA)

A 3D anatomic representation of the underlying cardiovascular geometry can provide the anatomic orientation needed for 3D flow visualization and retrospective flow quantification. The 4D flow data itself can be used to approximate the vascular geometry by generating a non-contrast 3D PC-MRA dataset without the need for an additional MRA acquisition. Based on PC-MRA applications in the early days of MRI (51), several strategies for the 4D flow based calculation of 3D PC-MRA data have been presented. In general, all techniques are based on identifying regions with high blood flow velocities in the phase difference images and suppression of background signal by signal intensities in the anatomical magnitude images (51,52). Although being a 'side product' of 4D flow MRI limited by spatial resolution, a 3D PC-MRA outline or transparent surface rendering of the vascular structures of interest (as shown in *Figures 2-9*) is greatly helpful for volumetric analysis and visualization.

Of note, non-contrast MRA examinations have gained increased interest after the occurrence of nephrogenic systemic fibrosis (NSF) and discovering a link to gadolinium-based MRA contrast agents (53). With the increasing temporal and spatial resolution of 4D flow MRI, better depiction of 3D PC angiograms and hemodynamic properties has already been demonstrated (54,55) and may become a useful alternative to contrast enhanced MRA.

Data analysis—3D blood flow visualization

For the qualitative evaluation of 4D flow MRI data, various options are available for 3D blood flow visualization (6,13,14,56-60). Most approaches use 2D analysis planes which are positioned in the vessel of interest. These analysis planes are used to emit 3D streamlines or time-resolved 3D pathlines for flow pattern visualization. 3D streamlines represent traces along the instantaneous 3D blood flow velocity vector field for an individual cardiac time-frame. For example, *Figures 2,5-7* illustrate the use of peak systolic 3D streamlines to visualize the spatial distribution and orientation of blood flow velocities. These examples illustrate the utility of 3D streamlines to identify specific systolic flow features such as outflow jets or helix flow. Color-coding by velocity magnitude facilitates the visual identification of regions with high systolic flow velocities.

For visualization of the temporal evolution of 3D blood flow over one or more heartbeats, time-resolved pathlines are the visualization method of choice. Color-coding of these traces allows for the visualization of velocity changes or to trace the flow pattern to its origin. Time-resolved pathlines are best viewed and displayed dynamically (movie mode) to fully appreciate the dynamic information and changes in blood flow over the cardiac cycle [see also supplemental *Video 1* illustrating the dynamics of 3D blood flow in a patient with bicuspid aortic valve (BAV) and aortic coarctation].

Data analysis—retrospective flow quantification

Comprehensive visualization of blood flow in a 3D

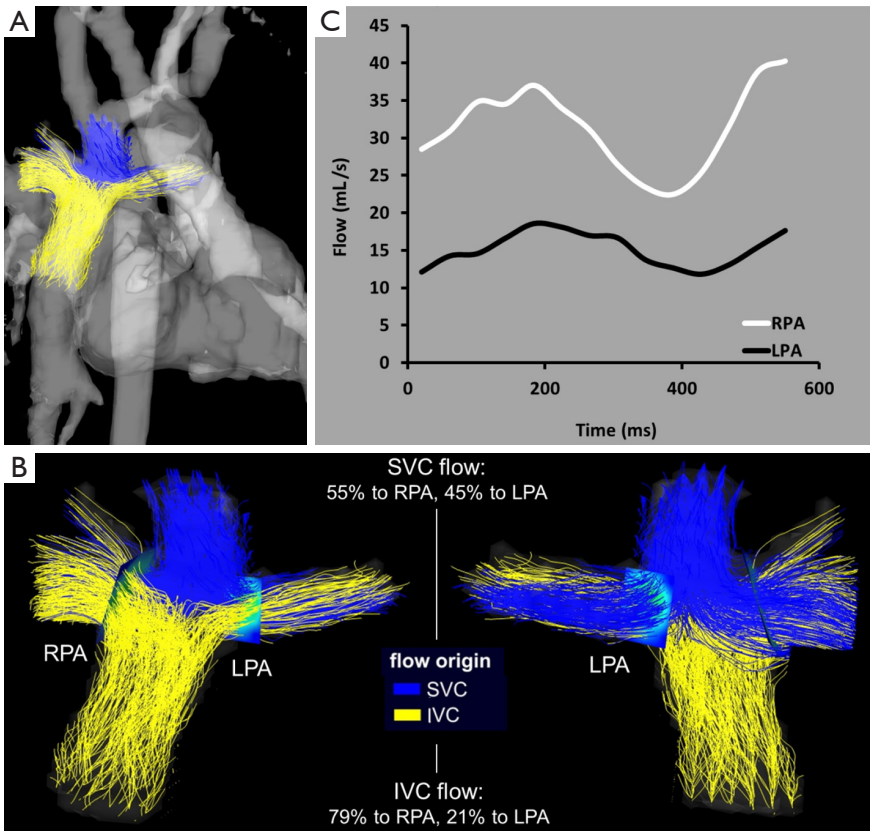

Figure 4 Flow analysis of 4D flow whole heart dataset in patient with Fontan circulation. (A) PC-MRA (grey) and pathlines (SVC-yellow, IVC-blue) visualize vascular anatomy and blood flow in the Fontan connection; (B) Mixing quantification shows relatively uniform distribution of SVC flow. However, flow from the IVC was predominately directed toward the RPA, indicating uneven distribution of hepatic-rich venous return from the lower body; (C) Flow quantification shows RPA flow is higher than LPA flow overall. SVC, superior vena cava; IVC, inferior vena cava; LPA/RPA, left/right pulmonary artery.

volume of interest enables a better understanding of the underlying pathologies, e.g., after a complex heart or aorta reconstruction surgery. The ability to perform additional quantitative analysis based on 4D flow MRI data has the potential to greatly impact diagnosis and patient management. In contrast to traditional 2D CINE PC-MRI, 4D flow MRI enables the retrospective quantification of hemodynamic parameters at any location within the 3D data volume at an offline workstation following acquisition (12,22,61). For the quantification of standard flow parameters, 2D analysis planes can be flexibly positioned in any artery or vein. The 3D PC-MRA data can be used to define the outline of the vessel lumen and subsequently calculate peak and mean velocities, total flow, net flow, or retrograde flow. Examples for the use of 4D flow MRI and retrospective quantification of flow-time curves, peak velocities or pressure gradients are shown in *Figures 2-9*.

A number of studies comparing 2D CINE PC-MRI and 4D flow MRI have shown excellent agreement for flow quantification (62,63). Furthermore, good scan-rescan reproducibility and low inter- and intra-observer variability of 4D flow MRI based flow quantification has been demonstrated for intracranial, cervical, thoracic and abdominal applications (23,62-64). It should be noted that a number of groups have presented strategies to assess more advanced hemodynamic parameters such as WSS, pressure difference, pulse wave velocity, TKE and others (20,22,24-29,31,65).

Clinical applications

In the last 15-20 years, 4D flow MRI acquisition and data

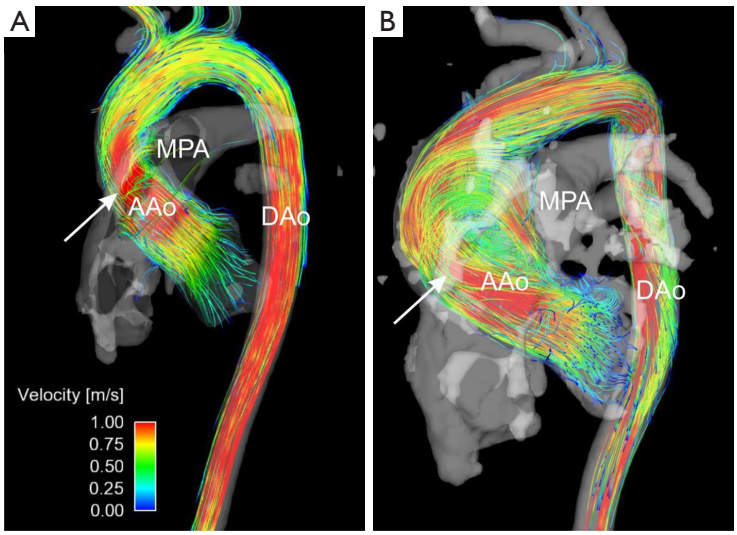

Figure 5 Two examples of systolic 3D streamline representation of 4D flow MRI data in patients with BAV. In both cases, a posteriorly directed high velocity flow jet is present in the ascending aorta suggesting aortic stenosis as a result of the BAV (white arrow). (A) BAV patient with minimal ascending aortic dilation; (B) BAV patient with a dramatically enlarged ascending aorta aneurysm with flow jet impingement. There is also a large amount of helical flow occurring within the aneurysm. This patient underwent valve-sparing ascending aorta repair. AAo, ascending aorta; MPA, main pulmonary artery; DAo, descending aorta; BAV, bicuspid aortic valve; MRI, magnetic resonance imaging.

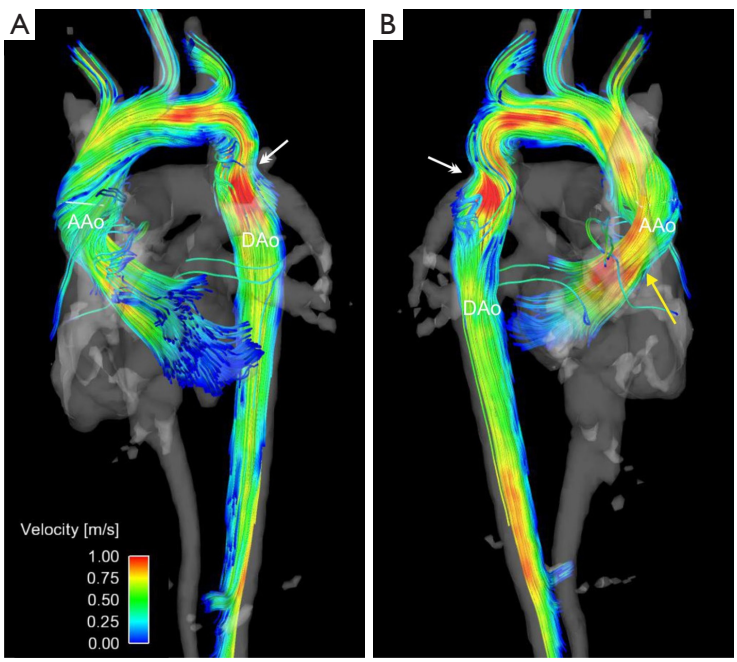

Figure 6 4D flow MRI in a 3.5-year-old pediatric patient with BAV and aortic coarctation at the distal arch/proximal descending aorta junction Systolic blood flow was visualized by 3D streamlines in anterior (A) and posterior (B) views demonstrating a high velocity flow jet in the ascending aorta and exaggerated right handed helical flow (yellow arrow). Note the significant flow derangement at the site of the coarctation with high velocity flow jets and throughout the region as well as non-laminar flow features both proximal and distal to coarctation (white double arrow). Using retrospective 4D flow MRI quantification, peak flow velocity in the mid-ascending aorta was found to be 1.16 m/s, while the post-coarctation peak velocity was measured at 1.34 m/s. BAV, bicuspid aortic valve; MRI, magnetic resonance imaging.

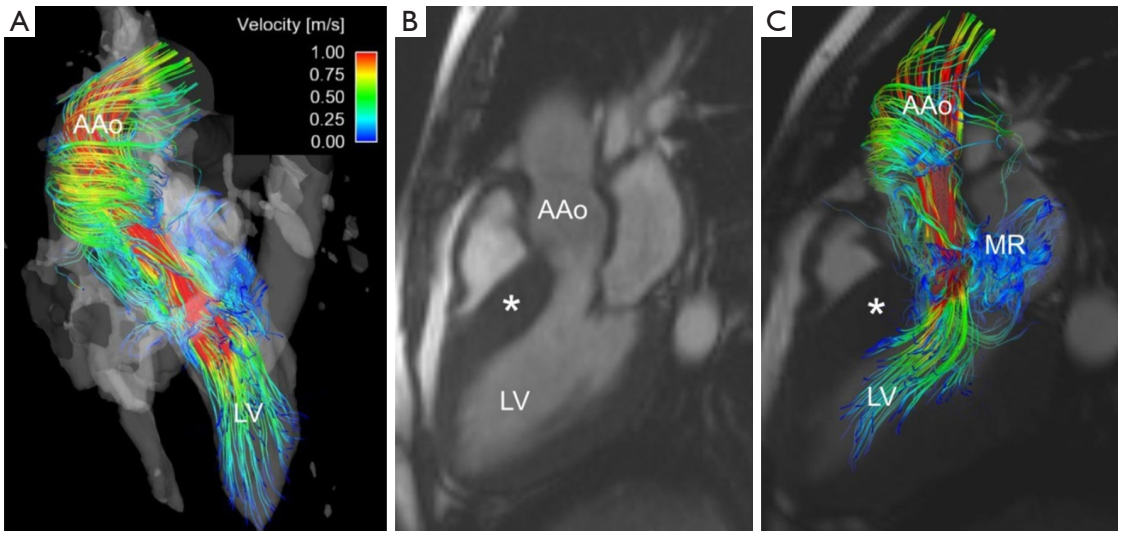

Figure 7 4D flow MRI in a patient with obstructive hypertrophic cardiomyopathy with thickening of the interventricular septum (*). (A) Systolic 3D streamlines in the anterior view shows an asymmetric flow jet in the left ventricular outflow tract as well as marked helical flow in the AAo; (B) end-diastolic frame of standard CINE SSFP MRI in three-chamber orientation in this patient demonstrating increased septal thickness; (C) co-registered 4D flow data with three-chamber SSFP cine image demonstrates the correlation between myocardial and vascular features and hemodynamic findings including the presence of MR. In this patient, LVOT pressure gradient assessed with MRI using the simplified Bernoulli equation was found to be 37.2 mmHg. AAo, ascending aorta; MR, mitral regurgitation; LVOT, left ventricular outflow tract.

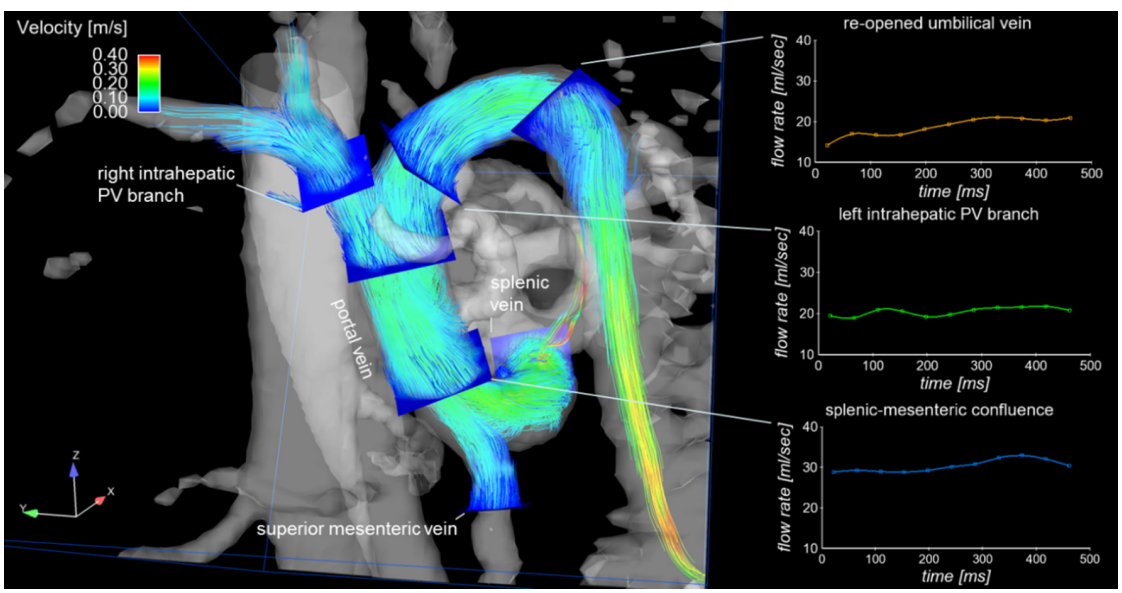

Figure 8 4D flow MRI visualization of the hepatic hemodynamics by 3D pathlines in a 50-year-old female patient with advanced liver cirrhosis Child-Pugh class B. Analysis planes were positioned in the splenic and superior mesenteric veins, splenic-mesenteric confluence, right and left intrahepatic portal vein branches and the proximal part of the portosystemic shunt represented by the umbilical vein. Pathlines reveal normal flow in the extrahepatic portal venous system. A reopening of the umbilical vein fed via the left branch of the intrahepatic portal vein is shown with an increase of flow velocity within the umbilical vein. Graphs on the right side show flow-time curves of the splenic-mesenteric confluence, left intrahepatic portal vein branch and the re-opened umbilical vein.

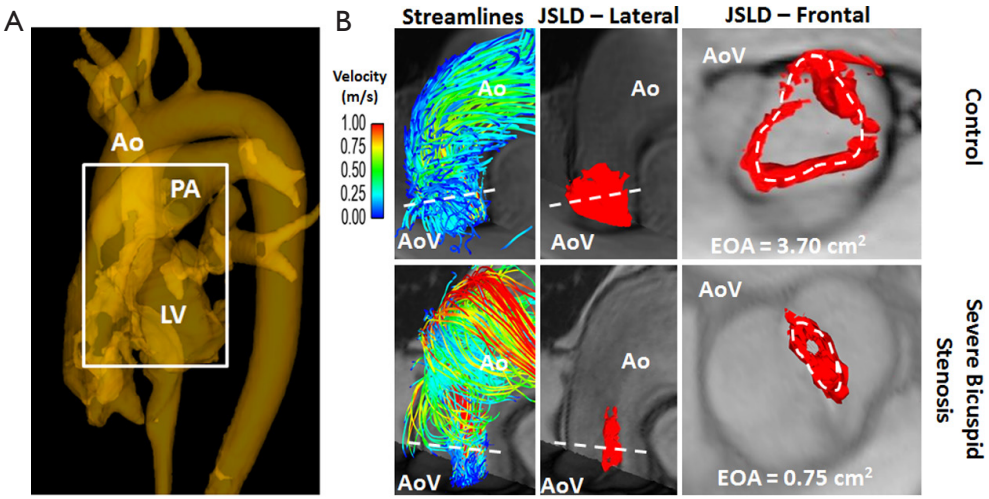

Figure 9 Aortic valve EOA estimation with the 4D flow jet shear layer detection method. (A) 3D PC-MRA based on 4D flow data. The white box delimits the volume for EOA assessment; (B) EOA estimation of a control subject (top row, EOA =3.70 cm^2) and a patient with severe bicuspid stenosis (bottom row, EOA =0.75 cm^2). 3D streamlines at peak systole indicate substantially different ascending aortic flow patterns for both subjects. The structures (red surfaces) result from flow JSLD computed from 4D flow MRI data at peak systole which can be employed to quantify changes in the aortic valve EOA, i.e., valve stenosis severity. The dashed white line indicates transvalvular maximal velocity position. Ao, aorta; AoV, aortic valve; LV, left ventricle; EOA, effective orifice area; JSLD, jet shear layer detection.

Video 1 The dynamics of 3D blood flow in a patient with bicuspid aortic valve and aortic coarctation.

analysis methods have been applied in a wide spectrum of clinical studies. Selected reports from the 4D flow MRI literature that present applications in different vascular territories in the human body are summarized in *Table 1*. In this article, we present a review of recent 4D flow MRI applications for the evaluation of congenital heart disease (CHD), the thoracic aorta, and hepatic and portal venous flow. Finally, the potential of new and more advanced metrics of cardiovascular hemodynamics that can be derived from 4D flow MRI data is briefly discussed. The authors would like to emphasize that the presented review of 4D flow applications is by no means complete. A comprehensive review of the many more applications of 4D flow MRI in the setting of different neurovascular and cardiovascular diseases, however, is beyond the scope of this article and the readers are referred to the literature.

Congenital heart disease (CHD)

When complex CHD (e.g., left or right hypoplastic heart syndrome, Tetralogy of Fallot (TOF), transposition of great arteries) is suspected, imaging evaluations provide clinicians with key diagnostic and surgical planning information. Thanks to advancements in pediatric cardiology and cardiovascular surgery, patients with complex cases of CHD are now living into adulthood (90). However, some patients develop serious complications and regular imaging evaluations are critical to their follow-up care.

The primary imaging modality used for the early evaluation and regular monitoring of patients with complex CHD is US, specifically transthoracic and transesophageal echocardiography (TTE and TEE) (90,91). Echocardiography is used routinely to assess functional impairment but has limitations, especially in older patients

Table 1 Selected applications of 4D flow MRI

Intracranial hemodynamics	
Bammer *et al*. (66) Ansari *et al*. (67)	Intracranial hemodynamics, Assessment of arteriovenous malformation
Meckel *et al*. (63)	Velocity comparison with ultrasound, 2D PC-MRI and 4D flow
Hope *et al*. (68)	Accelerated 4D flow of intracranial stenosis
Carotid arteries	
Schubert *et al*. (69), Harloff *et al*. (70)	Blood-flow pulsatility and patterns
Markl *et al*. (71)	Wall shear stress distribution
Whole heart	
Kilner *et al*. (59), Bolger *et al*. (72)	Flow through the heart
Wigström *et al*. (13), Ebbers *et al*. (26)	Particle trace visualization of intracardiac flow
Geiger *et al*. (73), François *et al*. (74)	Flow visualization and quantification in healthy volunteers and patients with TOF
Markl *et al*. (75), Bächler *et al*. (76), Nordmeyer *et al*. (64)	Flow visualization and quantification in healthy volunteers and patients with congenital heart disease
Thoracic aorta	
Kilner *et al*. (6), Hope *et al*. (77)	Helical and retrograde secondary flow patterns in the aortic arch
Bogren *et al*. (8), Markl *et al*. (75), Bürk *et al*. (78)	Thoracic aortic aneurysms and grafts
Bogren *et al*. (57)	Effects of age and coronary artery disease on blood flow in the thoracic aorta
Barker *et al*. (79), Hope *et al*. (80), Geiger *et al*. (81)	Wall sheer stress
Hope *et al*. (18), Frydrychowicz *et al*. (82)	Aortic coarctation and repair
Pulmonary arteries	
Tariq *et al*. (83)	Parallel imaging compressed sensing
Valverde *et al*. (12), Bächler *et al*. (84)	Flow quantification and visualization
Hepatic and portal venous flow	
Stankovic *et al*. (61,85,86)	4D flow MRI in the portal venous system, application for hemodynamic assessment in patients with liver cirrhosis; comparison to Doppler US
Frydrychowicz *et al*. (87)	Feasibility of PC VIPR in portal hypertension
Roldán-Alzate *et al*. (88)	Validation of PC VIPR 4D flow MRI for assessing the hemodynamics of portal hypertension
Renal arteries	
Francois *et al*. (54)	Visualization of segmental renal arteries and noninvasive assessment of hemodynamic significance of renal artery stenosis
Bley *et al*. (55)	Animal study with transstenotic pressure gradients derived from the velocity fields
Wentland *et al*. (62)	Repeatability and internal consistency of abdominal 2D and 4D
Peripheral vessels and peripheral arterial occlusive disease	
Frydrychowicz *et al*. (89)	Visualization of iliac and proximal femoral artery hemodynamics

due to their large body size and likelihood of having surgical scars. Thus, complementary imaging modalities are often needed, including catheter-based angiography, computed tomographic angiography (CTA) and MRI. In this cohort, whole heart 4D flow MRI techniques allow for a non-invasive comprehensive assessment of cardiovascular hemodynamics in the heart and surrounding great vessels. For this technique, the FOV is adjusted to contain the heart and surrounding large vessels to obtain flow data for the entire region in one imaging protocol. While scan times are longer due to the enlarged FOV (10-20 minutes depending on heart rate and respiration control efficiency), the main advantages of whole heart imaging are that it facilitates the systematic assessment of blood flow in multiple vessels and enables the retrospective analysis of any region of interest within the imaging FOV. Previous studies have shown that the technique can identify altered 3D flow characteristics related to the post-interventional status in patients with

CHD (73-75). 4D flow MRI also has the potential to predict or detect complications of CHD earlier in the disease course, which could impact outcomes through improved risk stratification and disease management in these patients.

In cases of severe hypoplastic left or right heart syndrome, patients with Fontan circulation have been evaluated for flow and mixing characteristics. 4D flow MRI has been used to acquire flow shunting in post-Fontan patients (75), and time-resolved pathlines were generated to illustrate the spatial distribution and dynamics of blood flow during the cardiac cycle. Visual and quantitative assessments showed varying total flow rates in each pulmonary artery (PA) as well as non-uniform mixing of blood to the left and right pulmonary arteries (LPA and RPA) for patients with Fontan (*Figure 4*). Fontan hemodynamics can thus be substantially different between patients despite similar Fontan geometry. Additionally, these findings indicate that some patients have uneven distribution of hepatic-rich venous return from the lower body to the left and right lungs (via the IVC), which has been suspected to influence the formation of serious complications of PA malformations and fistulas (92-95).

Related work has recently compared PC-MRI techniques. In healthy volunteers and patients with Fontan circulation, Bächler *et al*. (76) found agreement between flow shunting measurements based on 4D flow MRI pathline counting and 4D flow MRI net forward flow measurements, which served as the reference. Additionally, Valverde *et al*. (96) found agreement between flow shunting measurements by 4D flow MRI and by 2D PC-MRI in patients with systemic-to-pulmonary collateral flow.

4D flow whole heart MRI with 3D visualization and quantitative flow analysis has been performed in patients after TOF repair and marked variations in flow characteristics were observed (73,74). Findings included retrograde flow and vortex formation in the pulmonary trunk (PT) and PAs as well as higher RPA/LPA blood flow ratios, flow velocity and WSS in the PT than healthy volunteers. These results indicate the feasibility of the comprehensive evaluation of 3D hemodynamics by 4D flow MRI for the post-surgical assessment of patients with TOF.

Thoracic aorta

Some of the earliest and best studied applications of 4D flow MRI are the macroscopic visualization and 3D quantification of thoracic aorta hemodynamics (6,15,17,57,97). The study of aortic flow features has garnered a high degree of interest from both clinical and basic science researchers, in large part because it is well suited for fluid dynamic assessment and has been shown to provide clinically significant markers of disease. As discussed, the 3D velocity field acquisition in 4D flow not only allows for simple 2D planar calculations, but by using the appropriate visualization and quantification tools, a broad array of novel hemodynamic visualization and assessments can be performed in the thoracic aorta. These techniques include helical flow assessment, WSS analysis, flow jet eccentricity and a host of novel flow characteristics that are currently being explored (23,98). Additionally, the ability to visualize 3D flow features provides a potentially useful tool for clinicians and surgeons to use in planning treatment strategies and assessing response to interventions (99).

One particular area of clinical interest is patients with BAV who have an ascending aortic aneurysm or are at risk of aneurysm formations and dissection (*Figure 5*). There is an ongoing debate about the relative roles of genetically-induced vascular tissue changes and hemodynamic derangement as a result of the BAV in contributing to aneurysm formation and growth (100). While aortic stenosis does appear to put patients at a higher risk of aneurysm growth, no quantifiable hemodynamic parameters have been introduced that have found use as risk stratification markers, thus aneurysm size is the major branch point in treatment decisions in these patients (101). Recent data using 4D flow MRI has shown high velocity flow jets impinging on the ascending aortic wall and resulting in increased WSS in these regions (79,80,102), and additional results demonstrate increased helical flow in the ascending aorta of BAV patients (77). This type of assessment is unique to 4D flow MRI, and as further data is accumulated, MRI-measured WSS or jet impingement angle may help better risk-stratify BAV patients.

A second application of 4D flow MRI in the thoracic aorta is aortic arch and descending aorta assessment in patients with aortic coarctation (*Figure 6*). Aortic coarctation accounts for 6% of congenital cardiac malformations, is associated with hypertension and peripheral vascular disease, and often requires surgical repair (103). This disease is characterized by a congenital narrowing of the aorta, usually at the level of the distal arch or proximal descending aorta. To provide insight into the degree of stenosis and impact on distal flow as a result of the coarctation, traditional assessment includes aorta diameter measurements and post-coarctation flow velocity assessment. However, in

the majority of patients, these measures are difficult to obtain because of the tortuous nature of non-repaired coarctation. Using 4D flow MRI to assess this cohort of patients has proven to provide useful characteristics about the impact of coarctation and coarctation repair on flow features throughout the aorta (18,82). Patients with aortic coarctation tend to have flow jet eccentricity following the coarctation resulting in jet impingement along the descending aorta (104). Moreover, assessment with 4D flow allows for a comprehensive velocity assessment throughout the entire affected region near the coarctation (18). See also supplemental movie file illustrating the dynamics of 3D blood flow in a patient with BAV and aortic coarctation.

Additional thoracic aorta applications currently being explored include the impact of aortic flow features as a result of non-valvular cardiac disease such as hypertrophic cardiomyopathy (*Figure 7*) (105), assessment of hemodynamic variations resulting from surgical implants in ascending aorta aneurysm repair (7,106),and the correlation of retrograde flow in the aortic arch and descending aorta with cryptogenic ischemic stroke (107).

Hepatic and portal venous flow

Patients with liver cirrhosis develop a hyperdynamic syndrome with elevated heart rate and cardiac output and an increased splanchnic inflow (108). Advanced liver cirrhosis can cause increased hepatic resistance, reduced portal flow, elevated portal vein pressure gradients and portosystemic collateral vessels (109,110). Pharmacological and interventional therapies aim at reducing blood flow and consequently reduce the portal venous pressure (111). It is thus of clinical interest to quantitatively assess hepatic blood flow patterns.

Standard techniques for the assessment of liver blood flow and vascular architecture include Doppler US, contrast-enhanced low-dose multi-detector computed tomography (MDCT), 2D PC-MRI, contrast enhanced MR angiography (CE-MRA), or interventional wedged hepatic venous portography. All techniques, however, have specific limitations such as ionizing radiation and possible side effects of contrast application (112), limited anatomical coverage (113), poor observer variability (114) or invasiveness (115).

4D flow MRI with complete volumetric coverage of the venous and arterial liver vasculature may offer a new approach for the comprehensive characterization of liver morphology, 3D blood flow patterns and hemodynamic markers in patients with advanced liver cirrhosis (*Figure 8*). Pilot studies have demonstrated the feasibility of the technique for the assessment of hepatic blood flow with blood supply from the hepatic artery and the portal venous system (85). A study with liver cirrhosis patients validated the use of 4D flow MRI for portal venous flow quantification (maximum and mean velocities and flow volumes) compared to the reference standard data with Doppler US (61). In a small cohort of patients with advanced liver cirrhosis, regional flow quantification within the splanchnic system of the patients revealed an increased liver inflow in patients, but decreased outflow indicating the sensitivity of the methods to changes in liver hemodynamics (86).

Further studies demonstrated the utility of radial 4D flow MRI (PC VIPR) for the evaluation of hemodynamics with improved volumetric coverage of the entire hepatic and splanchnic vascular system with high spatial resolution (87,88). To better assess the range of different velocities in the high flow arterial system and the low flow portal venous system, a 5-point velocity-encoding technique was applied (38). Findings from these studies showed good internal consistency and inter- and intra-observer variability.

Promising future clinical applications include the assessment of shunt function in patients with advanced liver cirrhosis and interventional transjugular intrahepatic portosystemic shunt (TIPS) graft placement that are often difficult to assess with other non-invasive modalities (116). Functional imaging with 4D flow MRI may further develop in the area of clinical abdominal imaging in combination with morphological information about tissue structure derived from diffusion (117), perfusion (118) or elastography (119) MR imaging.

Advanced 4D flow hemodynamic markers

In addition to the retrospective quantification of blood flow, 4D flow data facilitates the evaluation of more advanced metrics of hemodynamics that are associated with complex blood flow patterns, such as highly helical flow commonly observed in the presence of aortic valve disease. Computation of advanced parameters capable of characterizing complex hemodynamic parameters includes the quantification of vorticity, helicity, flow angle, WSS, and turbulent and viscous energy loss. Previous studies have suggested that changes in these hemodynamic parameters may affect signalling and organization of endothelial cells. Cellular transduction of the hemodynamic properties may further induce functional changes within the cells by

altering multiple cell-signalling cascades via interaction with G-protein or kinase receptors as well as cell-surface-ion channels (120,121).

As an example, flow helicity is typically assessed using 3D flow visualization strategies such streamlines, flow vectors or time-resolved 3D pathlines. A more effective and representative analysis may be performed using vortical and helical flow-derived features. The direct estimation of effective orifice area (EOA) using a 4D flow jet shear layer detection (JSLD) method is an example of a vorticity-derived parameter (*Figure 9*). A recent sub-study of the multicenter SEAS study demonstrated that transvalvular energy loss, measured by echocardiography, may provide independent and additional prognosis information in asymptomatic AS patients, rather than conventional measures (122). In this context, recent studies proposed two methods, TKE dissipation and viscous energy losses (VEL), to compute energy loss using 4D flow MRI data. Both TKE and VEL may provide increased information compared to traditional energy loss computed with TTE. However, larger studies are needed to assess the diagnostic value of both parameters.

Discussion

4D flow MRI has been broadly applied in cardiovascular disease due to its ability to image vascular systems with full volumetric coverage and provide a comprehensive assessment of the vascular hemodynamics in a region of interest.

A limitation of 4D flow MRI is that scan times often are between 5 and 20 minutes, and are dependent on the breathing pattern and heart rate of the patient. Furthermore, limited spatial resolution restricts analyses in small vessels. Continued developments in sparse sampling techniques, e.g., compressed sensing (42) or radial acquisition (47), or multidimensional parallel imaging, e.g., k-t GRAPPA (39,123,124), might further improve the data acquisition and consecutive scan time. Another limitation of the technique is the need to acquire data over several cardiac cycles. This averaging over time potentially decreases peak velocity and flow measurements and cannot account for beat-to beat variations in blood flow.

An additional shortcoming of 4D flow MRI is that, for a majority of clinical studies that have explored the technique, limited numbers of patients or volunteers have been used. These smaller scale studies are needed for hypothesis generation and to select cohorts likely to benefit from the data 4D flow MRI can provide. Additionally, the technology and expertise required to implement 4D flow MRI is steadily increasing in a larger number of academic centers. As the technique filters out into the clinical research community, methodologies will be agreed upon and populations most likely to benefit will be identified, at which point larger scale trials should be performed. These large, multicenter cohort studies of are necessary to validate the added value of 4D flow MRI in the clinical setting.

Along with the need for larger studies, an additional barrier to the widespread clinical implementation of 4D flow MRI is the lack of validation against clinical gold standards in the case of the majority of clinical studies performed up to this point. Different studies have compared the technique to standard Doppler US in the intracranial vessel system (125), in the carotid arteries (70), in the thoracic aorta (82) and the hepatic system (61,85). The quantification results of these studies generally showed lower velocities with 4D flow MRI compared to Doppler US (61,70) with a moderate correlation between the methods. Studies comparing 2D CINE PC-MRI and 4D flow MRI studies have reported excellent agreement for flow quantification (62,63). For intracranial, cervical, thoracic and abdominal vascular territories, 4D flow MRI quantification has shown a good scan-rescan reproducibility and low inter- and intra-observer variability (23,62-64). However, most of the validation studies were either based on healthy volunteers or a limited number of patients with cardiovascular disease. Future clinical studies should evaluate the accuracy of quantitative 4D flow MRI relative to an independent flow quantification technique, e.g., invasive measurement of the blood flow parameters.

A further limitation of 4D flow MRI scan is the limited number of patients or volunteers in the clinical examination. This is partially related to the limited number of patients with rare diseases of the heart and cardiovascular system and partially due to the feasibility character of the studies. Large multicenter cohort studies of different diseases are needed to further validate the 4D flow MRI technique in the clinical setting. In this context, the limited availability of 4D flow MRI sequences, shortage of dedicated software packages, lack of standardized pre- and post-processing tools and limited processing of the large amount of acquired data within the current patient archive systems currently limit a broader clinical use, especially outside of academic centers.

A common effort is needed that will include manufacturers, researchers, and clinicians to work toward the increased availability and clinical adoption of 4D flow MRI. Future developments should include refining the clinical 4D flow

MRI workflow, determining the most useful ways to present the acquired data, enabling the data processing in the archive systems and streamlining the process of making the images and results available within the framework of the current patient data archive systems. A possible way might be the development of 3D labs with standardized processing tools and adapted resources for data processing.

In summary, 4D flow MRI has advanced over the last few years enabling the clinical application of the technique for comprehensive evaluation of cardiovascular blood flow in multiple organ systems and vascular territories. Future research efforts will improve the clinical applicability of 4D flow MRI and provide results in larger cohort studies. To date, a large number of studies have provided evidence that 4D flow MRI can help to better understand altered hemodynamics in patients with cardiovascular diseases and may help to improve patient management and monitoring of therapeutic response. The novel hemodynamic insights provided by 4D flow MRI are also likely to provide new risk stratification metrics in patients that have prognostic significance and can also impact individualized treatment decisions to optimize patient outcome.

Acknowledgements

Funding: NIH NHLBI grant R01HL115828; German Research Foundation (DFG) STA 1288/ 2-1.
Disclosure: The authors declare no conflict of interest.

References

1. Moran PR. A flow velocity zeugmatographic interlace for NMR imaging in humans. Magn Reson Imaging 1982;1:197-203.
2. Bryant DJ, Payne JA, Firmin DN, et al. Measurement of flow with NMR imaging using a gradient pulse and phase difference technique. J Comput Assist Tomogr 1984;8:588-93.
3. Nayler GL, Firmin DN, Longmore DB. Blood flow imaging by cine magnetic resonance. J Comput Assist Tomogr 1986;10:715-22.
4. Firmin DN, Nayler GL, Klipstein RH, et al. In vivo validation of MR velocity imaging. J Comput Assist Tomogr 1987;11:751-6.
5. Pelc NJ, Herfkens RJ, Shimakawa A, et al. Phase contrast cine magnetic resonance imaging. Magn Reson Q 1991;7:229-54.
6. Kilner PJ, Yang GZ, Mohiaddin RH, et al. Helical and retrograde secondary flow patterns in the aortic arch studied by three-directional magnetic resonance velocity mapping. Circulation 1993;88:2235-47.
7. Kvitting JP, Ebbers T, Wigström L, et al. Flow patterns in the aortic root and the aorta studied with time-resolved, 3-dimensional, phase-contrast magnetic resonance imaging: implications for aortic valve-sparing surgery. J Thorac Cardiovasc Surg 2004;127:1602-7.
8. Bogren HG, Mohiaddin RH, Yang GZ, et al. Magnetic resonance velocity vector mapping of blood flow in thoracic aortic aneurysms and grafts. J Thorac Cardiovasc Surg 1995;110:704-14.
9. Wigström L, Sjöqvist L, Wranne B. Temporally resolved 3D phase-contrast imaging. Magn Reson Med 1996;36:800-3.
10. Markl M, Chan FP, Alley MT, et al. Time-resolved three-dimensional phase-contrast MRI. J Magn Reson Imaging 2003;17:499-506.
11. Roes SD, Hammer S, van der Geest RJ, et al. Flow assessment through four heart valves simultaneously using 3-dimensional 3-directional velocity-encoded magnetic resonance imaging with retrospective valve tracking in healthy volunteers and patients with valvular regurgitation. Invest Radiol 2009;44:669-75.
12. Valverde I, Simpson J, Schaeffter T, et al. 4D phase-contrast flow cardiovascular magnetic resonance: comprehensive quantification and visualization of flow dynamics in atrial septal defect and partial anomalous pulmonary venous return. Pediatr Cardiol 2010;31:1244-8.
13. Wigström L, Ebbers T, Fyrenius A, et al. Particle trace visualization of intracardiac flow using time-resolved 3D phase contrast MRI. Magn Reson Med 1999;41:793-9.
14. Kozerke S, Hasenkam JM, Pedersen EM, et al. Visualization of flow patterns distal to aortic valve prostheses in humans using a fast approach for cine 3D velocity mapping. J Magn Reson Imaging 2001;13:690-8.
15. Bogren HG, Buonocore MH, Valente RJ. Four-dimensional magnetic resonance velocity mapping of blood flow patterns in the aorta in patients with atherosclerotic coronary artery disease compared to age-matched normal subjects. J Magn Reson Imaging 2004;19:417-27.
16. Markl M, Draney MT, Miller DC, et al. Time-resolved three-dimensional magnetic resonance velocity mapping of aortic flow in healthy volunteers and patients after valve-sparing aortic root replacement. J Thorac Cardiovasc Surg 2005;130:456-63.
17. Frydrychowicz A, Harloff A, Jung B, et al. Time-resolved, 3-dimensional magnetic resonance flow analysis at 3 T:

visualization of normal and pathological aortic vascular hemodynamics. J Comput Assist Tomogr 2007;31:9-15.
18. Hope MD, Meadows AK, Hope TA, et al. Clinical evaluation of aortic coarctation with 4D flow MR imaging. J Magn Reson Imaging 2010;31:711-8.
19. Markl M, Geiger J, Arnold R, et al. Comprehensive 4-dimensional magnetic resonance flow analysis after successful heart transplantation resolves controversial intraoperative findings and reveals complex hemodynamic alterations. Circulation 2011;123:e381-3.
20. Bock J, Frydrychowicz A, Lorenz R, et al. In vivo noninvasive 4D pressure difference mapping in the human aorta: phantom comparison and application in healthy volunteers and patients. Magn Reson Med 2011;66:1079-88.
21. Jiang J, Strother C, Johnson K, et al. Comparison of blood velocity measurements between ultrasound Doppler and accelerated phase-contrast MR angiography in small arteries with disturbed flow. Phys Med Biol 2011;56:1755-73.
22. Stalder AF, Russe MF, Frydrychowicz A, et al. Quantitative 2D and 3D phase contrast MRI: optimized analysis of blood flow and vessel wall parameters. Magn Reson Med 2008;60:1218-31.
23. Markl M, Wallis W, Harloff A. Reproducibility of flow and wall shear stress analysis using flow-sensitive four-dimensional MRI. J Magn Reson Imaging 2011;33:988-94.
24. Oshinski JN, Curtin JL, Loth F. Mean-average wall shear stress measurements in the common carotid artery. J Cardiovasc Magn Reson 2006;8:717-22.
25. Tyszka JM, Laidlaw DH, Asa JW, et al. Three-dimensional, time-resolved (4D) relative pressure mapping using magnetic resonance imaging. J Magn Reson Imaging 2000;12:321-9.
26. Ebbers T, Wigström L, Bolger AF, et al. Estimation of relative cardiovascular pressures using time-resolved three-dimensional phase contrast MRI. Magn Reson Med 2001;45:872-9.
27. Lum DP, Johnson KM, Paul RK, et al. Transstenotic pressure gradients: measurement in swine--retrospectively ECG-gated 3D phase-contrast MR angiography versus endovascular pressure-sensing guidewires. Radiology 2007;245:751-60.
28. Bolster BD Jr, Atalar E, Hardy CJ, et al. Accuracy of arterial pulse-wave velocity measurement using MR. J Magn Reson Imaging 1998;8:878-88.
29. Markl M, Wallis W, Brendecke S, et al. Estimation of global aortic pulse wave velocity by flow-sensitive 4D MRI. Magn Reson Med 2010;63:1575-82.
30. Dyverfeldt P, Sigfridsson A, Kvitting JP, et al. Quantification of intravoxel velocity standard deviation and turbulence intensity by generalizing phase-contrast MRI. Magn Reson Med 2006;56:850-8.
31. Dyverfeldt P, Gardhagen R, Sigfridsson A, et al. On MRI turbulence quantification. Magn Reson Imaging 2009;27:913-22.
32. Bernstein MA, Shimakawa A, Pelc NJ. Minimizing TE in moment-nulled or flow-encoded two- and three-dimensional gradient-echo imaging. J Magn Reson Imaging 1992;2:583-8.
33. Chai P, Mohiaddin R. How we perform cardiovascular magnetic resonance flow assessment using phase-contrast velocity mapping. J Cardiovasc Magn Reson 2005;7:705-16.
34. Bock J, Kreher BW, Hennig J, et al. Optimized pre-processing of time-resolved 2D and 3D Phase Contrast MRI data. 2007; Berlin, Germany. Abstract 3138.
35. Atkinson DJ, Edelman RR. Cineangiography of the heart in a single breath hold with a segmented turboFLASH sequence. Radiology 1991;178:357-60.
36. Thomsen C, Cortsen M, Sondergaard L, et al. A segmented K-space velocity mapping protocol for quantification of renal artery blood flow during breath-holding. J Magn Reson Imaging 1995;5:393-401.
37. Pelc NJ, Bernstein MA, Shimakawa A, et al. Encoding strategies for three-direction phase-contrast MR imaging of flow. J Magn Reson Imaging 1991;1:405-13.
38. Johnson KM, Markl M. Improved SNR in phase contrast velocimetry with five-point balanced flow encoding. Magn Reson Med 2010;63:349-55.
39. Baltes C, Kozerke S, Hansen MS, et al. Accelerating cine phase-contrast flow measurements using k-t BLAST and k-t SENSE. Magn Reson Med 2005;54:1430-8.
40. Moftakhar R, Aagaard-Kienitz B, Johnson K, et al. Noninvasive measurement of intra-aneurysmal pressure and flow pattern using phase contrast with vastly undersampled isotropic projection imaging. Ajnr 2007;28:1710-4.
41. Stadlbauer A, van der Riet W, Crelier G, et al. Accelerated time-resolved three-dimensional MR velocity mapping of blood flow patterns in the aorta using SENSE and k-t BLAST. European journal of radiology 2010;75:e15-21.
42. Lustig M, Donoho D, Pauly JM. Sparse MRI: The application of compressed sensing for rapid MR imaging. Magn Reson Med 2007;58:1182-95.
43. Ehman RL, Felmlee JP. Adaptive technique for high-definition MR imaging of moving structures. Radiology

1989;173:255-63.
44. Markl M, Harloff A, Bley TA, et al. Time-resolved 3D MR velocity mapping at 3T: improved navigator-gated assessment of vascular anatomy and blood flow. J Magn Reson Imaging 2007;25:824-31.
45. Uribe S, Beerbaum P, Sorensen TS, et al. Four-dimensional (4D) flow of the whole heart and great vessels using real-time respiratory self-gating. Magn Reson Med 2009;62:984-92.
46. Gu T, Korosec FR, Block WF, et al. PC VIPR: a high-speed 3D phase-contrast method for flow quantification and high-resolution angiography. Ajnr 2005;26:743-9.
47. Johnson KM, Lum DP, Turski PA, et al. Improved 3D phase contrast MRI with off-resonance corrected dual echo VIPR. Magn Reson Med 2008;60:1329-36.
48. Walker PG, Cranney GB, Scheidegger MB, et al. Semiautomated method for noise reduction and background phase error correction in MR phase velocity data. J Magn Reson Imaging 1993;3:521-30.
49. Bernstein MA, Zhou XJ, Polzin JA, et al. Concomitant gradient terms in phase contrast MR: analysis and correction. Magn Reson Med 1998;39:300-8.
50. Markl M, Bammer R, Alley MT, et al. Generalized reconstruction of phase contrast MRI: analysis and correction of the effect of gradient field distortions. Magn Reson Med 2003;50:791-801.
51. Dumoulin CL, Souza SP, Walker MF, et al. Three-dimensional phase contrast angiography. Magn Reson Med 1989;9:139-49.
52. Bernstein MA, Ikezaki Y. Comparison of phase-difference and complex-difference processing in phase-contrast MR angiography. J Magn Reson Imaging 1991;1:725-9.
53. Thomsen HS, Morcos SK, Dawson P. Is there a causal relation between the administration of gadolinium based contrast media and the development of nephrogenic systemic fibrosis (NSF)? Clin Radiol 2006;61:905-6.
54. François CJ, Lum DP, Johnson KM, et al. Renal arteries: isotropic, high-spatial-resolution, unenhanced MR angiography with three-dimensional radial phase contrast. Radiology 2011;258:254-60.
55. Bley TA, Johnson KM, Francois CJ, et al. Noninvasive assessment of transstenotic pressure gradients in porcine renal artery stenoses by using vastly undersampled phase-contrast MR angiography. Radiology 2011;261:266-73.
56. Napel S, Lee DH, Frayne R, et al. Visualizing three-dimensional flow with simulated streamlines and three-dimensional phase-contrast MR imaging. J Magn Reson Imaging 1992;2:143-53.
57. Bogren HG, Mohiaddin RH, Kilner PJ, et al. Blood flow patterns in the thoracic aorta studied with three-directional MR velocity mapping: the effects of age and coronary artery disease. J Magn Reson Imaging 1997;7:784-93.
58. Buonocore MH. Visualizing blood flow patterns using streamlines, arrows, and particle paths. Magn Reson Med 1998;40:210-26.
59. Kilner PJ, Yang GZ, Wilkes AJ, et al. Asymmetric redirection of flow through the heart. Nature 2000;404:759-61.
60. Markl M, Draney MT, Hope MD, et al. Time-resolved 3-dimensional velocity mapping in the thoracic aorta: visualization of 3-directional blood flow patterns in healthy volunteers and patients. J Comput Assist Tomogr 2004;28:459-68.
61. Stankovic Z, Csatari Z, Deibert P, et al. Normal and altered three-dimensional portal venous hemodynamics in patients with liver cirrhosis. Radiology 2012;262:862-73.
62. Wentland AL, Grist TM, Wieben O. Repeatability and internal consistency of abdominal 2D and 4D phase contrast MR flow measurements. Acad Radiol 2013;20:699-704.
63. Meckel S, Leitner L, Bonati LH, et al. Intracranial artery velocity measurement using 4D PC MRI at 3 T: comparison with transcranial ultrasound techniques and 2D PC MRI. Neuroradiology 2013;55:389-98.
64. Nordmeyer S, Riesenkampff E, Crelier G, et al. Flow-sensitive four-dimensional cine magnetic resonance imaging for offline blood flow quantification in multiple vessels: a validation study. J Magn Reson Imaging 2010;32:677-83.
65. Dyverfeldt P, Kvitting JP, Sigfridsson A, et al. Assessment of fluctuating velocities in disturbed cardiovascular blood flow: in vivo feasibility of generalized phase-contrast MRI. J Magn Reson Imaging 2008;28:655-63.
66. Bammer R, Hope TA, Aksoy M, et al. Time-resolved 3D quantitative flow MRI of the major intracranial vessels: initial experience and comparative evaluation at 1.5T and 3.0T in combination with parallel imaging. Magn Reson Med 2007;57:127-40.
67. Ansari SA, Schnell S, Carroll T, et al. Intracranial 4D flow MRI: toward individualized assessment of arteriovenous malformation hemodynamics and treatment-induced changes. AJNR Am J Neuroradiol 2013 ;34:1922-8.
68. Hope TA, Hope MD, Purcell DD, et al. Evaluation of intracranial stenoses and aneurysms with accelerated 4D flow. Magn Reson Imaging 2010;28:41-6.
69. Schubert T, Santini F, Stalder AF, et al. Dampening of

Blood-Flow Pulsatility along the Carotid Siphon: Does Form Follow Function? Ajnr 2011;32:1107-12.
70. Harloff A, Albrecht F, Spreer J, et al. 3D blood flow characteristics in the carotid artery bifurcation assessed by flow-sensitive 4D MRI at 3T. Magnetic Resonance in Medicine 2009;61:65-74.
71. Markl M, Wegent F, Zech T, et al. In vivo wall shear stress distribution in the carotid artery: effect of bifurcation geometry, internal carotid artery stenosis, and recanalization therapy. Circ Cardiovasc Imaging 2010;3:647-55.
72. Bolger AF, Heiberg E, Karlsson M, et al. Transit of blood flow through the human left ventricle mapped by cardiovascular magnetic resonance. J Cardiovasc Magn Reson 2007;9:741-7.
73. Geiger J, Markl M, Jung B, et al. 4D-MR flow analysis in patients after repair for tetralogy of Fallot. Eur Radiol 2011;21:1651-7.
74. François CJ, Srinivasan S, Schiebler ML, et al. 4D cardiovascular magnetic resonance velocity mapping of alterations of right heart flow patterns and main pulmonary artery hemodynamics in tetralogy of Fallot. J Cardiovasc Magn Reson 2012;14:16.
75. Markl M, Geiger J, Kilner PJ, et al. Time-resolved three-dimensional magnetic resonance velocity mapping of cardiovascular flow paths in volunteers and patients with Fontan circulation. Eur J Cardiothorac Surg 2011;39:206-12.
76. Bächler P, Valverde I, Pinochet N, et al. Caval blood flow distribution in patients with Fontan circulation: quantification by using particle traces from 4D flow MR imaging. Radiology 2013;267:67-75.
77. Hope MD, Hope TA, Meadows AK, et al. Bicuspid aortic valve: four-dimensional MR evaluation of ascending aortic systolic flow patterns. Radiology 2010;255:53-61.
78. Bürk J, Blanke P, Stankovic Z, et al. Evaluation of 3D blood flow patterns and wall shear stress in the normal and dilated thoracic aorta using flow-sensitive 4D CMR. J Cardiovasc Magn Reson 2012;14:84.
79. Barker AJ, Markl M, Burk J, et al. Bicuspid aortic valve is associated with altered wall shear stress in the ascending aorta. Circ Cardiovasc Imaging 2012;5:457-66.
80. Hope MD, Hope TA, Crook SE, et al. 4D flow CMR in assessment of valve-related ascending aortic disease. JACC Cardiovasc Imaging 2011;4:781-7.
81. Geiger J, Arnold R, Herzer L, et al. Aortic wall shear stress in Marfan syndrome. Magn Reson Med 2013;70:1137-44.
82. Frydrychowicz A, Markl M, Hirtler D, et al. Aortic hemodynamics in patients with and without repair of aortic coarctation: in vivo analysis by 4D flow-sensitive magnetic resonance imaging. Invest Radiol 2011;46:317-25.
83. Tariq U, Hsiao A, Alley M, et al. Venous and arterial flow quantification are equally accurate and precise with parallel imaging compressed sensing 4D phase contrast MRI. J Magn Reson Imaging 2013;37:1419-26.
84. Bächler P, Pinochet N, Sotelo J, et al. Assessment of normal flow patterns in the pulmonary circulation by using 4D magnetic resonance velocity mapping. Magn Reson Imaging 2013;31:178-88.
85. Stankovic Z, Frydrychowicz A, Csatari Z, et al. MR-based visualization and quantification of three-dimensional flow characteristics in the portal venous system. J Magn Reson Imaging 2010;32:466-75.
86. Stankovic Z, Csatari Z, Deibert P, et al. A feasibility study to evaluate splanchnic arterial and venous hemodynamics by flow-sensitive 4D MRI compared with Doppler ultrasound in patients with cirrhosis and controls. Eur J Gastroenterol Hepatol 2013;25:669-75.
87. Frydrychowicz A, Landgraf BR, Niespodzany E, et al. Four-dimensional velocity mapping of the hepatic and splanchnic vasculature with radial sampling at 3 tesla: a feasibility study in portal hypertension. J Magn Reson Imaging 2011;34:577-84.
88. Roldán-Alzate A, Frydrychowicz A, Niespodzany E, et al. In vivo validation of 4D flow MRI for assessing the hemodynamics of portal hypertension. J Magn Reson Imaging 2013;37:1100-8.
89. Frydrychowicz A, Winterer JT, Zaitsev M, et al. Visualization of iliac and proximal femoral artery hemodynamics using time-resolved 3D phase contrast MRI at 3T. J Magn Reson Imaging 2007;25:1085-92.
90. Kilner PJ. Imaging congenital heart disease in adults. Br J Radiol 2011;84 Spec No 3:S258-68.
91. Warnes CA, Williams RG, Bashore TM, et al. ACC/AHA 2008 guidelines for the management of adults with congenital heart disease: a report of the American College of Cardiology/American Heart Association Task Force on Practice Guidelines (Writing Committee to Develop Guidelines on the Management of Adults With Congenital Heart Disease). Developed in Collaboration With the American Society of Echocardiography, Heart Rhythm Society, International Society for Adult Congenital Heart Disease, Society for Cardiovascular Angiography and Interventions, and Society of Thoracic Surgeons. J Am Coll Cardiol 2008;52:e143-263.
92. Hiramatsu T, Komori S, Nishimura Y, et al. Conversion

from Total Cavopulmonary Shunt to Fontan Circulation: Improved Cyanosis with an 11-Year Interval. Ann Thorac Cardiovasc Surg 2008;14:29-31.
93. Sernich S, Ross-Ascuitto N, Dorotan J, et al. Surgical Improvement of Hepatic Venous Mixing to Resolve Systemic Arterial Hypoxemia Associated with Post-Fontan Pulmonary Arteriovenous Fistulae. Texas Heart Institute Journal 2009;36:480-2.
94. Shah MJ, Rychik J, Fogel MA, et al. Malformations After Superior Cavopulmonary Connection: Resolution After Inclusion of Hepatic Veins in the Pulmonary Circulation. Ann Thorac Surg 1997;63:960 -3.
95. Shinohara T, Yokoyama T. Pulmonary Arteriovenous Malformation in Patients with Total Cavopulmonary Shunt: What Role Does Lack of Hepatic Venous Blood Flow to the Lungs Play? Pediatr Cardiol 2001;22:343-6.
96. Valverde I, Nordmeyer S, Uribe S, et al. Systemic-to-pulmonary collateral flow in patients with palliated univentricular heart physiology: measurement using cardiovascular magnetic resonance 4D velocity acquisition. J Cardiovasc Magn Reson 2012;14:25.
97. Bogren HG, Buonocore MH. 4D magnetic resonance velocity mapping of blood flow patterns in the aorta in young vs. elderly normal subjects. J Magn Reson Imaging 1999;10:861-9.
98. Barker AJ, Bandi KC, Garcia J, et al. eds. A Direct Calculation of Hemodynamic Energy Loss in the Presence of Abnormal Aortic Flow. Salt Lake City, UT, 2013.
99. Clough RE, Waltham M, Giese D, et al. A new imaging method for assessment of aortic dissection using four-dimensional phase contrast magnetic resonance imaging. J Vasc Surg 2012;55:914-23.
100. Bonow RO. Bicuspid aortic valves and dilated aortas: a critical review of the ACC/AHA practice guidelines recommendations: Am J Cardiol. 2008;102:111-4.
101. Bonow RO, Carabello BA, Chatterjee K, et al. 2008 focused update incorporated into the ACC/AHA 2006 guidelines for the management of patients with valvular heart disease: a report of the American College of Cardiology/American Heart Association Task Force on Practice Guidelines (Writing Committee to revise the 1998 guidelines for the management of patients with valvular heart disease). Endorsed by the Society of Cardiovascular Anesthesiologists, Society for Cardiovascular Angiography and Interventions, and Society of Thoracic Surgeons. J Am Coll Cardiol 2008;52:e1-142.
102. Bieging ET, Frydrychowicz A, Wentland A,et al. In vivo three-dimensional MR wall shear stress estimation in ascending aortic dilatation. J Magn Reson Imaging 2011;33:589-97.
103. Abbruzzese PA, Aidala E. Aortic coarctation: an overview. J Cardiovasc Med (Hagerstown) 2007;8:123-8.
104. Allen BD, Barker AJ, Carr JC, et al. Time-resolved three-dimensional phase contrast MRI evaluation of bicuspid aortic valve and coarctation of the aorta. Eur Heart J Cardiovasc Imaging 2013;14:399.
105. Allen B, Barker A, Collins J, et al. eds. Hemodynamic assessment of obstructive hypertrophic cardiomyopathy using 4D flow MRI. Salt Lake City, UT, 2013.
106. Bogren HG, Buonocore MH, Follette DM. Four-dimensional aortic blood flow patterns in thoracic aortic grafts. J Cardiovasc Magn Reson 2000;2:201-8.
107. Markl M, Kilner PJ, Ebbers T. Comprehensive 4D velocity mapping of the heart and great vessels by cardiovascular magnetic resonance. J Cardiovasc Magn Reson 2011;13:7.
108. Groszmann RJ. Hyperdynamic circulation of liver disease 40 years later: pathophysiology and clinical consequences. Hepatology 1994;20:1359-63.
109. Bosch J, Garcia-Pagan JC. Complications of cirrhosis. I. Portal hypertension. J Hepatol 2000;32:141-56.
110. Garcia-Tsao G. Portal hypertension. Curr Opin Gastroenterol 2000;16:282-9.
111. Abraldes JG, Tarantino I, Turnes J, et al. Hemodynamic response to pharmacological treatment of portal hypertension and long-term prognosis of cirrhosis. Hepatology 2003;37:902-8.
112. Van Beers BE, Leconte I, Materne R, et al. Hepatic perfusion parameters in chronic liver disease: dynamic CT measurements correlated with disease severity. AJR Am J Roentgenol 2001;176:667-73.
113. Yzet T, Bouzerar R, Allart JD, et al. Hepatic vascular flow measurements by phase contrast MRI and doppler echography: a comparative and reproducibility study. J Magn Reson Imaging 2010;31:579-88.
114. de Vries PJ, van Hattum J, Hoekstra JB, et al. Duplex Doppler measurements of portal venous flow in normal subjects. Inter- and intra-observer variability. J Hepatol 1991;13:358-63.
115. Ripoll C, Groszmann R, Garcia-Tsao G, et al. Hepatic venous pressure gradient predicts clinical decompensation in patients with compensated cirrhosis. Gastroenterology 2007;133:481-8.
116. Stankovic Z, Blanke P, Markl M. Usefulness of 4D MRI flow imaging to control TIPS function. Am J Gastroenterol 2012;107:327-8.
117. Taouli B, Koh DM. Diffusion-weighted MR imaging of

the liver. Radiology 2010;254:47-66.
118. Annet L, Materne R, Danse E, et al. Hepatic flow parameters measured with MR imaging and Doppler US: correlations with degree of cirrhosis and portal hypertension. Radiology 2003;229:409-14.
119. Taouli B, Ehman RL, Reeder SB. Advanced MRI methods for assessment of chronic liver disease. AJR Am J Roentgenol 2009;193:14-27.
120. Lehoux S, Tedgui A. Cellular mechanics and gene expression in blood vessels. J Biomech 2003;36:631-43.
121. Balachandran K, Sucosky P, Yoganathan AP. Hemodynamics and mechanobiology of aortic valve inflammation and calcification. Int J Inflam 2011;2011:263870.
122. Bahlmann E, Gerdts E, Cramariuc D, et al. Prognostic value of energy loss index in asymptomatic aortic stenosis. Circulation 2013;127:1149-56.
123. Griswold MA, Jakob PM, Heidemann RM, et al. Generalized autocalibrating partially parallel acquisitions (GRAPPA). Magn Reson Med 2002;47:1202-10.
124. Jung B, Stalder AF, Bauer S, et al. On the undersampling strategies to accelerate time-resolved 3D imaging using k-t-GRAPPA. Magn Reson Med 2011;66:966-75.
125. Meckel S, Stalder AF, Santini F, et al. In vivo visualization and analysis of 3-D hemodynamics in cerebral aneurysms with flow-sensitized 4-D MR imaging at 3 T. Neuroradiology 2008;50:473-84.

Cite this article as: Stankovic Z, Allen BD, Garcia J, Jarvis KB, Markl M. 4D flow imaging with MRI. Cardiovasc Diagn Ther 2014;4(2):173-192. doi: 10.3978/j.issn.2223-3652.2014.01.02

